Biosensors and Bioelectronics 146 (2019) 111726

Contents lists available at ScienceDirect

Biosensors and Bioelectronics

journal homepage: http://www.elsevier.com/locate/bios

Rapid and reagentless detection of thrombin in clinic samples via microfluidic aptasensors with multiple target-binding sites

Neng Yu, Jianmin Wu *

Department of Chemistry, Zhejiang University, Hangzhou, 310058, China

ARTICLE INFO

Keywords:
RIFS
Thrombin detection
Open-ended porous silicon (OEPSi)
Aptamer
Multiple binding-site

ABSTRACT

A reusable and straightforward aptasensor with the implementation of open-ended porous silicon (OEPSi) membranes was introduced for thrombin detection. When passing through the nanochannels of OEPSi integrated in a microfluidic cell, thrombin in sample solution could be captured by thrombin-binding aptamers (TBA) immobilized along the inner walls. The formation of thrombin-aptamer complex causes refractive index changes which can be measured by reflective interferometric Fourier transform spectroscopy (RIFTS). And this flow-through configuration with OEPSi has proven more efficient in capturing thrombin than the flow-over configuration with closed-ended PSi. For higher sensitivity, we investigated how the pore size, ionic strength, pH and aptamers affected the thrombin-aptamer interaction in nanopores. Under optimized conditions, the limits of detection (LOD) for thrombin detection in the buffer and serum were ~6.70 nM and ~8.21 nM respectively and a wide linear detection range (10–1000 nM) was observed. More importantly, this work reveals the sensitivity of the label-free biosensor can be significantly improved by attaching newly designed aptamers with two thrombin-binding sites. This phenomenon also indicates the potential of aptamer probes in adjusting effective pore size and enhancing the interaction between aptamers and targets through meticulous sequence design. Furthermore, the proposed strategy has been applied in thrombin detection in clinic samples successfully, which was verified by Enzyme-Linked Immunosorbent Assays (ELISA).

1. Introduction

Thrombin, a serine protease, regulates blood coagulation and catalyzes many related reactions in the human body. As the dominating proteinase in the clotting cascade, thrombin can convert soluble fibrinogen to insoluble fibrin to prevent bleeding. Under normal circumstances, thrombin is not present in the blood. But if blood vessels are damaged, prothrombin would be activated by Factor X (Xa) and turn into thrombin rapidly. The thrombin concentration can reach nanomolar or micromolar level during the coagulation process (Shuman and Majerus, 1976). The occurrence of some diseases such as thrombosis (Sambrano et al., 2001), atherosclerosis (Kalz et al., 2014), and Alzheimer's (Tripathy et al., 2013) also correlates with overexpression or abnormality of thrombin. Moreover, it has been reported that thrombin is able to induce the growth, metastasis, and angiogenesis of tumors (Nierodzik and Karpatkin, 2006). Therefore, rapid detection of thrombin in clinic samples attracts the growing interest in clinic diagnosis.

Immunoassays are one of the most commonly used approaches for thrombin detection. Recently, aptamers serve as affinity ligands increasingly and are regarded as promising alternatives as the role of antibodies in bioanalysis. Aptamers are single-strand oligonucleotides (15–60 nts) with high binding affinity to specific target molecules. They are isolated from random oligonucleotide libraries through iterative selection-amplification processes named Systematic Evolution of Ligands by Exponential Enrichment (SELEX). The targets of aptamers range from metal ions (DasGupta et al., 2015), small organic molecules (De Stefano et al., 2006; Modh et al., 2017), proteins (Zou et al., 2012; Sze et al., 2017), cells (Sun et al., 2018) to bacteria (Urmann et al., 2016; Majdinasab et al., 2018). The affinity constants of aptamers lie between the micromolar or nanomolar scale, close to those of antibodies to antigens (Jenison et al., 1994). Compared to antibodies, aptamers have more unique features, including reversible folding, small size, ease of chemical modification, simple chemical synthesis, and excellent stability.

Similar to antibody-antigen pair, the binding event between aptamers and target molecules can not naturally output signal without the help of signal reporters. Although fluorescent labeling and electrochemical strategies have been widely employed in aptamer-based

* Corresponding author.
E-mail address: wjm-st1@zju.edu.cn (J. Wu).

https://doi.org/10.1016/j.bios.2019.111726
Received 3 August 2019; Received in revised form 18 September 2019; Accepted 20 September 2019
Available online 23 September 2019

sensing (Xiao et al., 2005; Lin et al., 2006), label-free methods still show several superior features. For example, they can monitor the binding event between aptamers and analytes in real time. Among various label-free methods, nanopore technology has attracted wide attention because of its high sensitivity and selectivity. Up to now, aptamers have been introduced in nanopore biosensors increasingly (Guo et al., 2015; Jiang et al., 2017). They can enter nanopore channels and immobilize on the inner walls. Owing to the small size (d~2 nm) and low molecular weight (6–30 kDa), aptamers can lower the blank signal in label-free detection and thereby increase the sensitivity. Another advantage of using aptamers in nanopore technology is their tunable sequence and structure, which can conveniently regulate effective pore size in nanopore sensing and adjust the binding kinetics as well as strength. Binding of aptamers with target analytes can induce the blockage of nanopore channels and result in the reduction of ionic flux current or changes in optical signal (Urmann et al., 2015). In this way, this interaction can be readout by electrical or optical signals.

Porous silicon (PSi) films combined with reflective interferometric spectroscopy (RIFS) as a label-free optical transducer is highly sensitive to refractive index change upon the binding events in the porous layer, which is attributed to the Fabry-Perot fringe shifts from reflect interference of light from the top and bottom interfaces of a PSi film. Compared to other types of nanopore materials, the main advantages of PSi are its versatile surface modification, adjustable pore size, easy fabrication, and biocompatibility (Canham, 1995). Previous work has shown superior performance of PSi as the sensing material in RIFS (Lin et al., 1997; Pacholski et al., 2005). However, PSi interferometers for biosensing suffer from limited application in clinic diagnosis due to poor sensitivity (Vilensky et al., 2015). In a typical sensing system, closed-ended PSi membranes worked in a flow-over format are usually employed. In this flow-over scheme, sample solution straightly goes over the PSi pores, resulting in the limited mass transport and poor binding of analytes to receptors along the walls. To solve this problem, Weiss and co-workers (Zhao et al., 2016b) proposed a flow-through strategy to help affinity probes attached on nanopore channels to bind with targets more efficiently. Other methods to improve sensitivity of PSi interferometric biosensors have been also developed. For example, pre-concentrating targets using electrokinetic isotachophoresis (ITP) was adopted to improve sensing performance (Arshavsky-Graham et al., 2017). Barillaro and co-workers (Mariani et al., 2016) found another way, namely optimizing signal processing algorithm, to push the detection limitation down to 20 pM. More recently, this group proposed a layer-by-layer electrostatic assembly of oppositely-charged polyelectrolytes method to eliminate nonspecific adsorption and achieved the low detection limitation at femtomolar level (Mariani et al., 2018). For nanopore-based sensor, the interplay between affinity probes (eg. aptamer) and nanopore channels plays an important role in the sensing performance, however, this issue has not been investigated.

Herein, we fabricated a cost-effective and highly sensitive microfluidic optical sensor incorporating an electrochemically etched PSi film detached from the silicon substrate. The open-ended porous silicon (OEPSi) film attached with thrombin-binding aptamer (TBA) can successfully work in the flow-through mode and capture thrombin efficiently. After optimizing the pore size, TBA length, as well as solution chemistry, the limit of detection (LOD) of the OEPSi biosensor could reach nanomolar level, which is close to electrochemical and other optical transducing strategies (Table S1). Moreover, the performance of the sensing device could be further improved through sequence design of aptamer. Owing to the synergetic effect of molecular filtration of OEPSi films and designable binding-sites of TBA, the biosensor displays high sensitivity and selectivity for thrombin detection in clinical serum samples.

2. Materials and methods

2.1. Materials and reagents

NaCl, $MgCl_2$, $CaCl_2$, NaOH, HF (40%), H_2SO_4 (98%), aqueous H_2O_2 solution (30%), and absolute ethanol was purchased from Sinopharm Chemical Reagent Co., Ltd. HF (HPLC), N'-(ethylcarbonimidoyl)-N, N-dimethylpropane-1,3-diamine monohydrochloride (EDC), and N-hydroxysuccinimide (NHS) was obtained from Aladdin Co., (China). (3-Aminopropyl) triethoxysilane (APTES) was purchased from Sigma-Aldrich Chemicals. Thrombin was purchased from Yeasen Biotech Co., Ltd and thrombin Enzyme-Linked Immunosorbent Assay (ELISA) kit was bought from Gelatins Co., (Shanghai, China). Insulin was bought from Duly Co.,(Nanjing, China). All oligonucleotides functionalized with carboxyl groups at 5′ ends, albumin from bovine serum (BSA), and TE buffer (10 mM Tris-HCl, 1 mM EDTA, pH = 8.0) were bought from Sangon Biotech (Shanghai) Co., Ltd. (China). Human serum was collected from healthy people (Zhejiang University Hospital, China) with ethical committee permission and diluted tenfold with TE buffer (140 mM NaCl, 10 mM $MgCl_2$, 5 mM KCl, 10 mM Tris-HCl, 1 mM EDTA, pH = 7.0). Below is the sequence of all oligonucleotides used in this work:

TBA-15: 5′–HOOC–TTTTTTTTTTGGTTGGTGTGGTTGG-3'.

TBA-29: 5′–HOOC–TTTTTTTTTTAGTCCGTGGTAGGGCAGGTTGGGGTGACT-3'.

Random Sequence: 5′–HOOC–TTTTTTTTTTAATTGGTGTGGTTAA-3'.

D-TBA: 5′–HOOC–TTTTTTTTTTGGTTGGTGTGGTTGGTTTTTTTTTTGGTTGGT-GTGGTTGG -3'.

2.2. PSi-based aptasensor fabrication

An aptamer@OEPSi membrane was fixed between a PDMS microfluidic channel (~10 mm × 10 mm × 3 mm) and a PMMA cell (Scheme 1a, d = 4 cm, thickness = 1 cm). The upper channel included the inlet for sample loading while the outlet lay in the bottom PMMA cell. These two channels constituted a flow-through cell where the sample solution can pass through the OEPSi channels vertically. The diameter of the free-standing area of OEPSi membrane is approximately 4 mm after it is mounted between two channels by blue tack. For the flow-over scheme, a PSi chip was fixed between a PMMA slice and a stainless platform as reported in the previous work (Tang et al., 2013). All solution was introduced from an injection syringe forced by a syringe pump (PHD, 2000; Harvard Co.,). OEPSi membranes are fragile and must be handled with care. So, the flow rate remained 5 μL/min for avoiding additional pressure and ensuring the stability of PSi films in this study.

2.3. Reflectometric interference spectroscopy and data analysis

All interferometric reflectance spectra were obtained from an Ocean Optics USB 2000 + CCD spectrometer. The light came from a tungsten halogen lamp (LS-1, Ocean Optics) and was focused on the center of the OEPSi layer (spot size = 1 mm^2) through a bifurcated fiber-optic cable. One arm of the fiber-optic cable was connected to the spectrometer for monitoring spectra and the other one was linked to the tungsten halogen lamp. The spectrum data was recorded automatically at a spectral acquisition time of 100 m s and in the wavelength from 400 to 1000 nm by OOIBase32. All spectra were analyzed by the IGOR program through Fast Fourier Transform (FFT) and the corresponding effective optical thickness (EOT) was determined by the Fabry-Perot relationship:

$$EOT = 2nL = m\lambda$$

where n is the average refractive index of the PSi layer including its contents, L is the thickness of the PSi membrane, λ refers to the

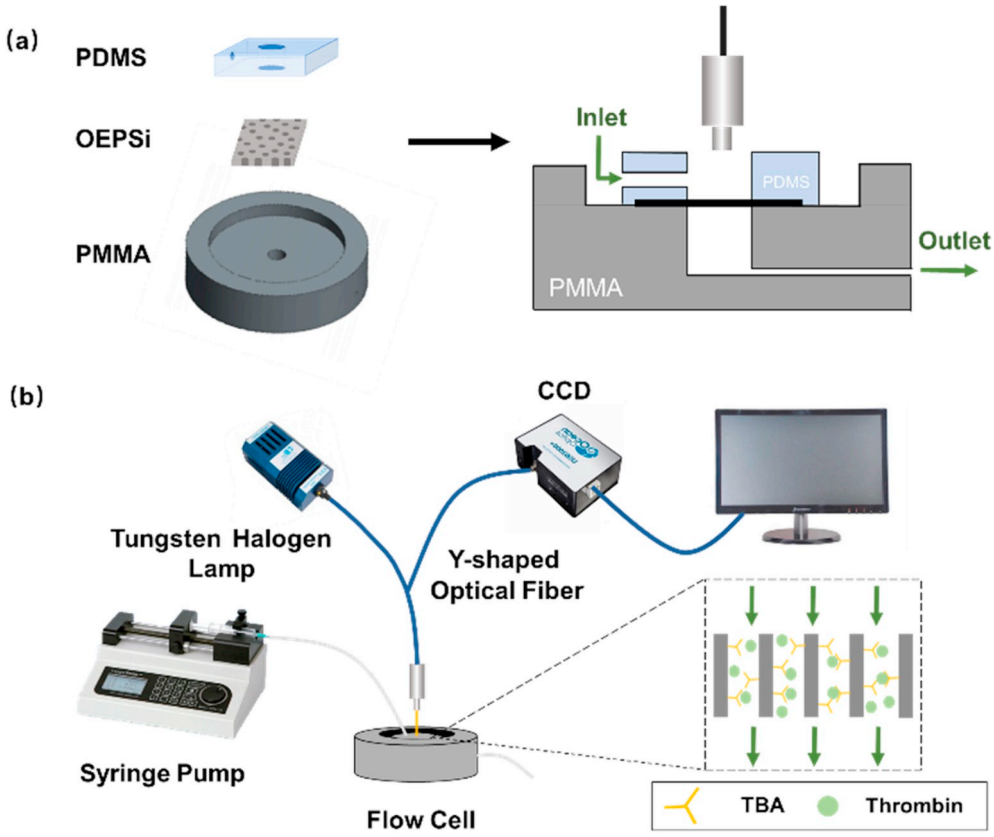

Scheme 1. Schematic illustration of the aptamer@OEPSi sensor fabrication (a) and the sensing mechanism (b) for thrombin detection.

wavelength of maximum constructive interference for a spectral fringe of order m. In this work, the signal response was presented as the relative EOT shift which was defined in the following equation:

$$\text{Signal Response} = \Delta EOT \Big/ EOT_0 = \frac{EOT_{sample} - EOT_{buffer}}{EOT_{buffer}} \times 100\%$$

where EOT_{sample} is the average EOT value obtained from the saturation phase of the sample solution and EOT_{buffer} refers to the average EOT value obtained from the baseline of TE buffer (all running buffer in this work was TE buffer).

3. Results and discussion

3.1. Characterization of PSi

In this study, OEPSi membranes were fabricated by electrochemical etching and removing from the silicon wafer subsequently as described in Supplementary Information. It can be seen in Fig. S1 that the thickness of the OEPSi membranes is around 19.9 μm and the diameter of nanopore is 14.9 nm. Then PSi nanochannels were biofunctionalized with TBA as the recognition surface of the sensor. The immobilization of TBA was realized through covalent coupling: freshly made OEPSi layers were firstly oxidized by Piranha solution, and then incubated with APTES/EtOH solution for silanization. Finally, the binding between TBA functionalized with carboxyl groups and OEPSi was performed through EDC/NHS chemistry. For ensuring the G-quadruplex configuration of TBA, there are 10-mer polyT tails at the 5' ends as the linkage sequence. The modified PSi was characterized by Diffuse Reflectance Infrared Fourier Transform Spectroscopy (DRIFT) as illustrated in Fig. S2. The DRIFT spectra confirm the success of aptamer immobilization. The triple peaks at ~2100 cm^{-1} are the absorption band of Si-H_x bond (x = 1,2,3) in freshly made OEPSi. After oxidization, the peaks of Si-H_x bond are absent, but the absorption band assigned to the O–H vibration of silanol groups at 3743 cm^{-1} and the strong absorption band of Si–O–Si bond at around 1200 cm^{-1} appear. The peaks at 2870 and 2943 cm^{-1} belong to the stretching vibration of the C–H bond in the silanized PSi. Importantly, the double peaks at 1540 and 1645 cm^{-1} belonging to characteristic peaks of carbonyl groups are clear evidence of successful immobilization of TBA.

3.2. Feasibility test of the aptamer@OEPSi biosensor

The detection principle of the proposed sensor is displayed in Scheme 1b. Thrombin in given dimensions of 8.8 nm × 6.8 nm × 6.1 nm (Sze et al., 2017) would be captured by aptamers bound to OEPSi inwalls when flowing through channels, leading to the refractive index increase of the PSi layer. In this study, we chose relative EOT changes as the signal response for eliminating batch-to-batch variation of thickness. Nonetheless, EOT shifts may be attributed to two factors: generation of thrombin-aptamer complex and filling of thrombin into nanochannels. To confirm the function of aptamers, random sequence oligonucleotides with the same length as 15-mer TBA were employed as the blank control. From Fig. 1, upon loading 100 nM thrombin, the optical signal generated from the blank control is negligible in comparison with TBA. This phenomenon proves the binding between aptamers and thrombin plays a pivotal role in signal generation. And the signal response changes little after rinsing by TE buffer, which illustrates optical signals from non-specific binding is not distinguishable. Thus, no rinsing steps are required for further experiments.

3.3. Condition optimization

For aptamer-based biosensors, the recognition of target molecules is crucial to the sensing performance. The interaction between aptamers and thrombin is affected by many factors, for example, the binding

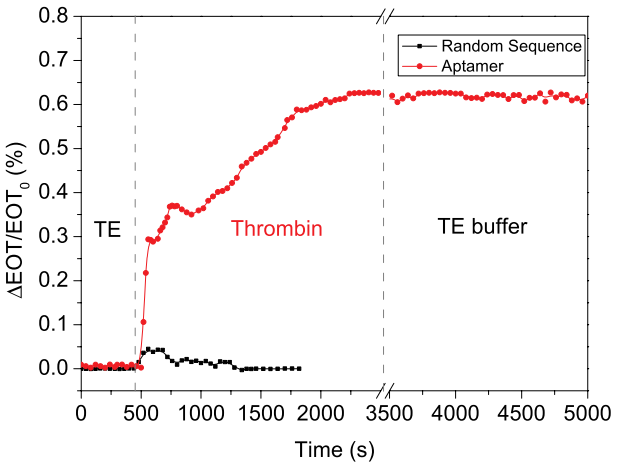

Fig. 1. Sensing behaviors of the OEPSi detection platform modified with 15-mer TBA (red) and random sequence (black) after introducing 100 nM thrombin in TE buffer. (For interpretation of the references to colour in this figure legend, the reader is referred to the Web version of this article.)

affinity, pore morphology and buffer. Herein, the experimental parameters, including pore size, pH, ionic strength and aptamers were optimized for improving the sensitivity of the optical sensor in this section.

3.3.1. Aptamers

The most principle and direct parameter should be the binding affinity of aptamers. In thrombin detection, two aptamers are widely used with different sequence, structure and dissociation constant (K_d). The 15-mer aptamers (5′-GGTT GGTGTGGTTGG-3′) have a rather weak binding affinity with the K_d of ~100 nM. The 15-mer TBA would form a G-quadruplex structure when binding to the fibrinogen-recognition site of thrombin. The other 29-mer TBA (5′-AGTCCGTGGTAGGG-CAGGTTGGGGTGACT-3′) can bind to the heparin-binding site of thrombin with an internal G-quadruplex structure like chairs, but the affinity is higher (K_d = 0.5 nM) (Tasset et al., 1997). Though 29-mer TBA has a stronger binding ability, the performance of TBA-15 (15-mer TBA+ 10-mer PolyT) as recognition probes in the OEPSi biosensor is better than TBA-29 (29-mer TBA+ 10-mer PolyT) in Fig. 2a. The cause might be the dimensions of thrombin is comparable to the diameter of nanopores so larger size of aptamers means smaller effective pore size, which probably hinders the sample flow. Therefore, both binding affinity and effective pore size are of great importance in nanopore sensing. And all aptamers used in the following experiments were TBA-15 for higher sensitivity.

3.3.2. pH

Electrolyte pH has a substantial influence on the sensitivity of aptasensors. Through protonation and deprotonation, pH variation has a direct effect on the electronegativity of aptamers, which is related to the electrostatic repulsion between aptamers and target analytes. The

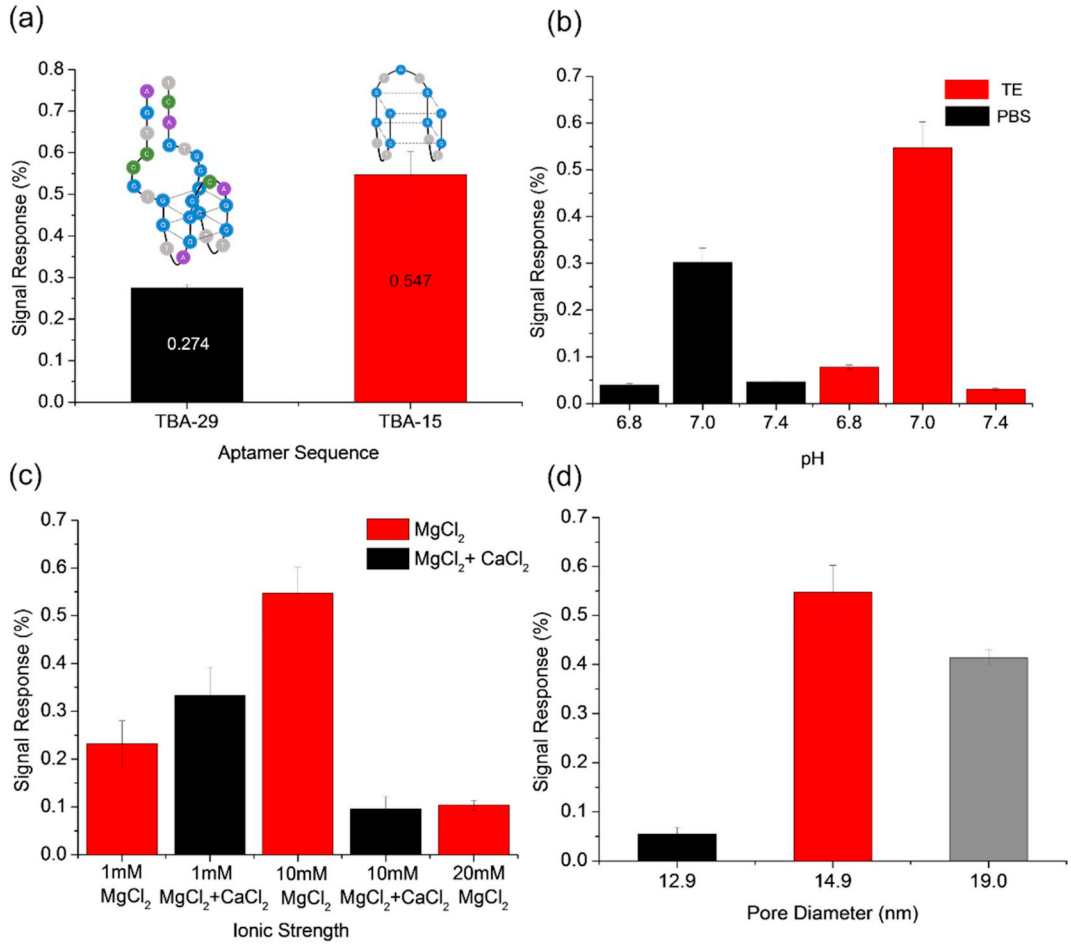

Fig. 2. The detection performance of the OEPSi biosensor upon loading of 100 nM thrombin: (a) PSi functionalized with TBA-15 (red) and TBA-29 (black). (b) at the pH values of 6.8, 7.0 and 7.4 in TE buffer (red) and PBS buffer (black). (c) with various concentrations of $MgCl_2$ and $CaCl_2$ in TE buffer (from left to right: 1 mM $MgCl_2$,1 mM $MgCl_2$+1 mM $CaCl_2$, 10 mM $MgCl_2$, 10 mM $MgCl_2$+10 mM $CaCl_2$, 20 mM $MgCl_2$). (d) PSi with different pore size (d = 12.9, 14.9 and 19.0 nm). (For interpretation of the references to colour in this figure legend, the reader is referred to the Web version of this article.)

isoelectric point (pI) of 15-mer TBA is approximately 4.1 (Tan et al., 2017) and that of thrombin is 7.0–7.6 (W et al., 1979). For PSi-based sensors, a pH value closed to the pI value of targets is the best choice (Chen and Sailor, 2011; Arshavsky-Graham et al., 2017). To investigate the optimal electrolyte pH for thrombin-aptamer interaction, we chose three different pH values: 6.8, 7.0 and 7.4 in TE buffer (140 mM NaCl, 10 mM $MgCl_2$, 5 mM KCl) and PBS buffer (137 mM NaCl, 2.7 mM KCl, 10 mM Na_2HPO_4, 2 mM KH_2PO_4, 10 mM $MgCl_2$). We can see in Fig. 2b that the neutral solution is more favorable for thrombin-aptamer interaction than the acid and the alkaline solution in both cases. At this pH value, better performance in TE buffer can be explained by stability of aptamers.

3.3.3. Ionic strength

Metal cations are able to weaken the electronegativity of aptamers, which contributes to the binding performance (Tan et al., 2017). Apart from K^+ and Na^+, alkaline-earth metal ions like Mg^{2+} and Ca^{2+} are also usually involved in the buffer for aptasensors. The previous study has proven the presence of divalent cations induces self-organized conformation changes of aptamers (Tan and Chen, 2006) and improves their binding affinity (Girardot et al., 2012; Tan et al., 2017). For instance, Mg^{2+} ions are beneficial to the formation of the duplex secondary structure of oligonucleotides (Yunlong and Qiang, 2017) and 29-mer TBA conformation changes because of emerging of heterogeneous binding sites (Girardot et al., 2010). On the contrary, the effect of Ca^{2+} ions for thrombin-TBA interaction has not been fully understood. Herein, this work utilized an RIFS platform to investigate the thrombin-TBA binding in TE buffer (140 mM NaCl, 5 mM KCl, pH = 7.0) with different divalent ionic strength. In Fig. 2c, Mg^{2+} displays a concave upward tendency in the concentration from 1 mM to 20 mM. The addition of Ca^{2+} at the same concentration increased the binding at the low concentration (1 mM). Instead, at the higher concentration (20 mM) it attenuates the interaction signals. Because the increase of Mg^{2+} can reduce the electronegativity of aptamers, the excess of Mg^{2+} ions will lead to the competitive binding of aptamers between thrombin and Mg^{2+}. Similarly, the small addition of Ca^{2+} ions helps to enhance the thrombin-aptamer interaction, but excessive Ca^{2+} ions have a shielding effect.

3.3.4. Pore size

Analyte transport from the bulk solution to PSi inner walls is a function of pore dimensions. Small pores could provide higher sensitivity and signal response (Kant et al., 2014). But the electrostatic repulsion between thrombin-aptamer complex along the wall and thrombin in bulk solution is also influential in the further binding of thrombin and aptamers when the size of thrombin is comparable to the pore diameter. As a result, the biosensing performance could be optimized by tuning nanopore size. Three OEPSi films etched under the current density of 5,30 and 50 mA/cm^2 respectively were studied to find out the optimum pore size for TBA-15. SEM images (Fig. S1a and Fig. S3) show the surface morphology of these films with the pore diameter of around 12.9, 14.9 and 19.0 nm respectively. The analytical performance of three aptasensors with different nanopore size is present in Fig. 2d. It could be observed that the PSi film with ~14.9 nm pore size achieves the best sensing performance. This result indicates the binding between aptamers and targets is poor in too large or small nanopores. In large pores, the chance of aptamer-target binding is too low to generate distinct optical response, whereas electrostatic repulsion dominates the binding reaction in the small channels.

3.3.5. Optimized protocol

According to the above-mentioned results, OEPSi membranes functionalized with TBA-15 with a diameter of 14.9 nm and TE buffer with 10 mM $MgCl_2$ at pH = 7.0 were employed in further experiments as the optimal parameters.

3.4. Comparison of PSi sensors in the flow-through and flow-over scheme

Porous materials are favorable sinks for protein binding in aptasensors because the absorption kinetics predominantly depends on the flux into the porous cavities (Lazzara et al., 2011). The diffusion of large molecules like protein is determined not only by intrinsic properties but also the geometry, like pore size (Mu et al., 2007; Kant et al., 2014), depth (Lazzara et al., 2011; Kant et al., 2014) and structure (Zhao et al., 2016a, 2016b) of porous materials. In most cases, single-ended pores are widely utilized in biosensing devices, while study about open-ended pores in biosensing is still in its infancy. However, because of limited mass transport, most of the analytes sweep the channels without interacting with sensing areas in the flow-over configuration, which results in long response time and massive sample consumption. In contrast, the flux diffusion rate in the flow-through configuration is calculated to be 3000 times faster than in the flow-over configuration (Zhao et al., 2016b).

To compare the efficiency of two configurations, flow-through and flow-over PSi sensors with open-ended and closed-ended pores respectively were fabricated. The PSi chips used in the flow-over scheme (Fig. 3b) were prepared similarly just without removing from wafers. As shown in Fig. 3c, this flow-through approach does speed up biosensing and improve the sensing performance. The response time in the flow-through mode was only a third of that in the flow-over mode owing to efficient analyte delivery. The signal response in the flow-through mode was nearly two times as high as the flow-over mode, probably because more target analytes could transport to sensing surface and interact with aptamers driven by strong mass transfer effect in the flow-through configuration. As seen, this result is in line with the conclusion of Weiss's group (Zhao et al., 2016a), but in their work, the preparation of open-ended silicon nanopore films needs more complex microfabrication steps.

3.5. Thrombin detection using TBA-15 (single binding-site probes) in buffer

Under optimal experiment conditions, quantitative detection of thrombin in buffer was performed. As seen in Fig. 4a, a linear correlation ($R^2 = 0.996$) between thrombin concentration and the optical response was obtained in the range of 10–1000 nM. The corresponding linear equation was $\Delta EOT/EOT_0\ (\%) = 0.00450 c_{thrombin}\ (nM) + 0.1209$ and the limit of detection of the OEPSi sensor in TE buffer was 6.70 nM (3σ, $\sigma_{TE} = 0.0110\%$). This result reveals the analytical performance of our platform is comparable to other methods (Table S1) in thrombin detection. For example, Derkus and colleagues (Derkus et al., 2016) developed an impedimetric aptasensor for thrombin detection in blood samples with a discrete detection range (6.25–250 nM and 0.5–10 μM) and a LOD of 6.25 nM. Umrao et al. (2018) reported a fluorescent aptasensor for measuring thrombin in the low concentration range (LOD = 8.9 pM). In consideration of both detection limitation and range, our study is better than some work for clinic diagnosis (Table S1).

BSA and insulin were selected as control groups to check the protein selectivity. The selectivity of the aptasensor could result from both high specificity of aptamers and size exclusion effect of nanopores. In Fig. 4b, there are no obvious EOT changes for the sensor after interacting with BSA nor insulin. The transport of BSA into nanopores is greatly restricted because of its large size and aggregation (Li et al., 2016), which confirms the filtering effect of PSi nanopores. But insulin is much smaller than thrombin, so insulin trials proves the selectivity of aptamers.

3.6. Regeneration of OEPSi biosensors

The property of aptamers, reversible folding, brings the feasibility of repeated use to our device. Aiming at weakening the aptamer-target binding and washing out thrombin, 2 M NaCl aqueous solution was applied as the dissociation buffer after the saturation phase of thrombin.

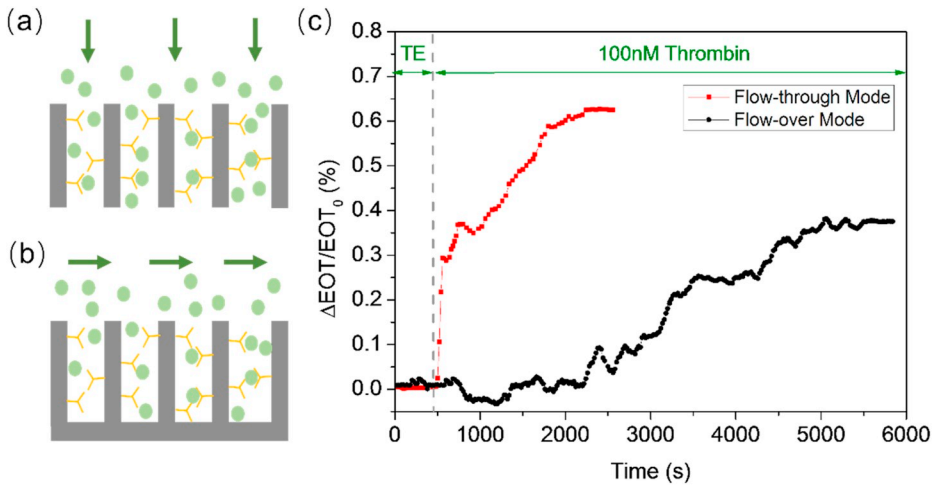

Fig. 3. Schematic illustration of PSi sensors in the flow-through (a) and flow-over (b) configuration. (c) Comparison of responding curves from the PSi sensors in the flow-over (black) and flow-through (red) mode during the injection of 100 nM thrombin. Both trials were conducted under optimal experimental conditions. (For interpretation of the references to colour in this figure legend, the reader is referred to the Web version of this article.)

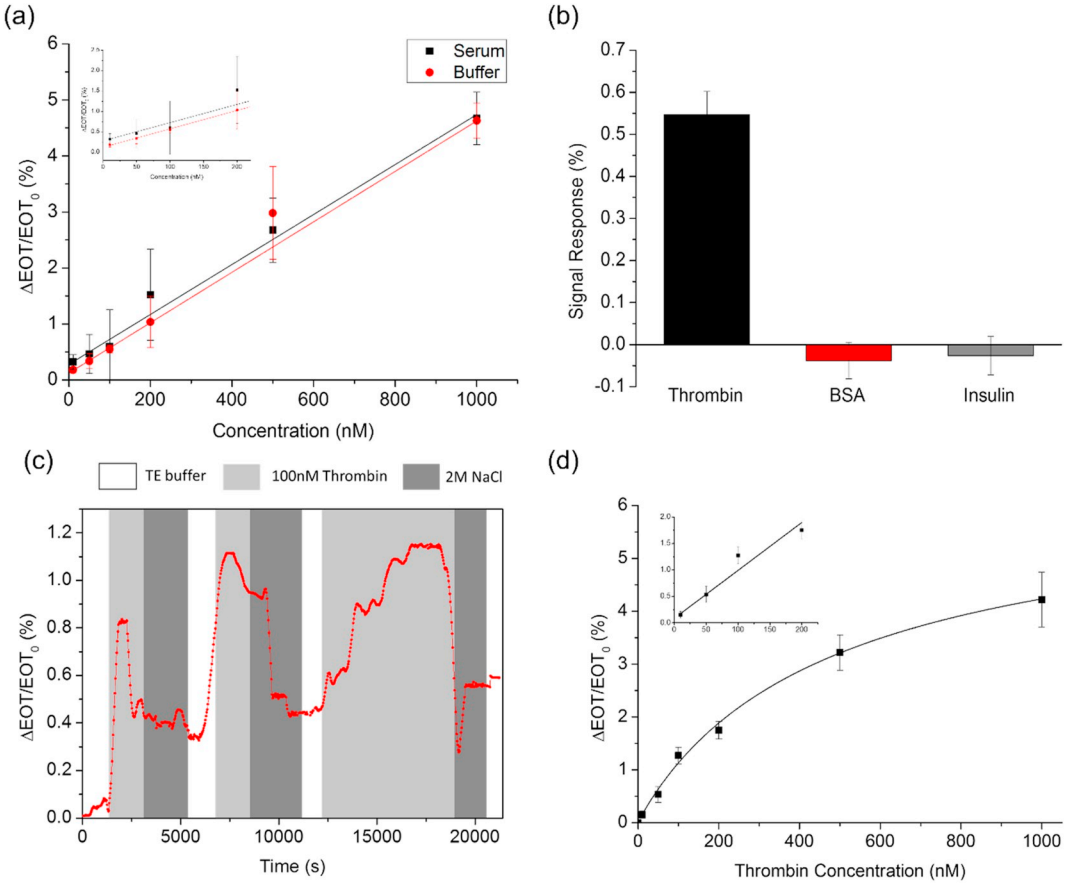

Fig. 4. (a) Calibration curves obtained from the OEPSi sensor with single binding-site for thrombin (10–1000 nM) detection in TE buffer (red) and 10% human serum (black). Inset: zoomed-in calibration curves in the range of low concentration (10–200 nM). (b) Protein selectivity assessment of the OEPSi aptasensor in thrombin (37.4 kDa, black), BSA (66.4 kDa, red) and insulin (5.8 kDa, grey) samples at the concentration of 100 nM. (c) Regeneration of the OEPSi biosensor: TE buffer firstly flowed into the detection system as the baseline. Subsequently, 100 nM thrombin (in TE buffer) was injected. After the saturation phase, 2 M NaCl solution was applied as the dissociation buffer. The cycle of capture and release was repeated for three times and the flow rate remained 5 μL/min. (d) Calibration curve of the OEPSi sensor with dual binding-sites for thrombin detection (10–1000 nM) in 10% serum. Thrombin was spiked in 10% human serum diluted by TE buffer. The inset is the linear fitting curve in the low concentration range (10–200 nM). (For interpretation of the references to colour in this figure legend, the reader is referred to the Web version of this article.)

The three cycles of capture, elution and re-capture were present in Fig. 4c, so we can see the OEPSi biosensor can be regenerated easily and rapidly by elution of high concentration salt (%CV = 5.8%). The regeneration behaviors of the aptasensor indicate its potential in the commercial application with low cost. The baselines for the first cycle and the follow-up cycles were slightly different because irreversible sites were occupied at first.

3.7. Thrombin detection using single binding-site probes in serum

To evaluating sensing performance in clinical application, thrombin measurement in serum was taken. For the OEPSi sensor with single binding-site, the relative EOT changes increase when the thrombin level goes up with a good linear relationship ($R^2 = 0.996$), as displayed in Fig. 4d. The fitted curve equation is $\Delta EOT/EOT_0\ (\%) = 0.00446c_{thrombin}$ (nM) +0.2773 with a LOD of 8.21 nM (3σ, $\sigma_{TE} = 0.0134\%$). It is noted that the calibration plot in serum is almost overlapped to that in buffer. So, it can be inferred the matrix effect in serum is nearly negligible in thrombin detection owing to open-ended channels.

3.8. Thrombin detection using dual binding-sites probes in serum

Undoubtedly, the sensitivity of the proposed sensor is related to the aptamer density along the PSi walls. However, aptamer density is restricted by the stereo-hindrance effect. For further improving the sensitivity, DNA receptors with two thrombin-binding sites (D-TBA) were tried. There were two 15-mer TBA sequences in a D-TBA probe with adequate spatial separation (10 bases). The corresponding relationship between thrombin level in serum and $\Delta EOT/EOT_0$ (Fig. 4d) can be described in the following logistic equation:

$$\text{Response} = 6.3792 - \frac{6.375}{1 + \left(\frac{c_{thrombin}}{494.016}\right)^{0.960}} \quad (R^2 = 0.993)$$

In low concentration range (10–200 nM), there was a good linear correlation between signal response and thrombin concentration: $\Delta EOT/EOT_0\ (\%) = 0.00960c_{thrombin}$ (nM)+0.06383 ($R^2 = 0.944$). The LOD was calculated to be 2.17 nM (3σ, $\sigma_{TE} = 0.00615\%$). So additional thrombin-binding sites on probes can significantly improve the sensitivity of the sensor (2.2 times) at low concentration. Briefly, additional binding-sites are likely to conjugate with more thrombin and reduce the effective pore size. To some extent, smaller effective size of nanopores implies higher possibilities of collision between target molecules and probes on the surface. This result suggests that fine-tuning of aptamer sequence offers the possibility of precisely controlling effective nanopore diameters. However, for high thrombin concentration the OEPSi sensor with the dual-site aptamer reached saturation more easily. This phenomenon can be explained by spatial effect and different recognition modes of target-aptamer complex. Because the thrombin-aptamer pair may have a strong electrostatic repulsion to further binding of adjacent aptamers to thrombin at high concentration. Besides, there are two anion exosites on thrombin, which means TBA may interact with both sites forming sandwich-like structure (Wang and Liu, 2009).

3.9. Recovery assays and accuracy certification

Based on the calibration curves, recovery assays of thrombin (10,50 and 100 nM) in 10% serum were performed with three replicates. The recovery rates of samples are 92.7%–105.7% for single binding-site mode and 91.8%–105.8% for dual binding-sites mode with a relative standard deviation (RSD) less than 10% as listed in Table S2. In order to check the accuracy of the proposed strategy, ELISA which is known as the golden standard of thrombin measurement were undertaken. Fig. 5 depicts that the data obtained from ELISA is nearly overlapped with that obtained from the RIFS aptasensor. The one-way Analysis of Variance (ANOVA) suggests no significant difference between the proposed sensor in both modes and ELISA ($P > 0.05$).

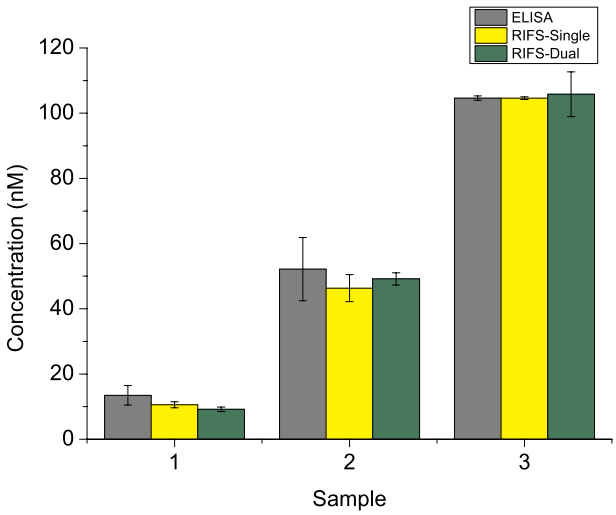

Fig. 5. Correlation of the proposed RIFS sensor in the single and dual binding-site modes with ELISA for thrombin detection in 10% human serum (three replicates).

4. Conclusions

The present work fabricated a RIFS microfluidic biosensor for thrombin detection based on aptamer@OEPSi membranes prepared in a straightforward and low-cost way. The OEPSi films detached from electrochemically etched silicon could act as nanofiltration film and signal transducer simultaneously. By controlling the pore size of OEPSi, the membrane could allow the target molecule, thrombin, to infiltrate into the pore channel and bind with TBA attached on the inner wall of pore channel. In this way, the effective optical thickness of the membrane could selectively respond to the concentration of thrombin either in standard or serum samples. Compared to the flow-over mode of a conventional RIFS biosensor, the flow-through configuration displayed higher sensitivity and fast response rate. When dual binding-sites on TBA probes were introduced, the sensitivity almost doubled. We believe that, in a nanopore sensor, the rational design of aptamer structure could remarkably regulate the molecular interaction and significantly enhance the biosensing capability owing to the spatial confinement effect, although more extensive work needs to be conducted in the future. The combination of well-designed aptamer and OEPSi membrane provide a simple, reusable, sensitive and accurate sensing platform for clinical laboratory diagnosis.

Declaration of competing interest

The authors declare that they have no known competing financial interests or personal relationships that could have appeared to influence the work reported in this paper.

CRediT authorship contribution statement

Neng Yu: Conceptualization, Methodology, Investigation, Formal analysis, Software, Validation, Writing - original draft. **Jianmin Wu:** Supervision, Writing - review & editing.

Acknowledgement

This work is supported by the National Science Foundation of China (Nos. 21575127 and 21874118).

Appendix A. Supplementary data

Supplementary data to this article can be found online at https://doi.org/10.1016/j.bios.2019.111726.

References

Arshavsky-Graham, S., Massad-Ivanir, N., Paratore, F., cheperT, S., Bercovici, M., Segal, E., 2017. ACS Sens. 2, 1767–1773.
Canham, L.T., 1995. Adv. Mater. 7, 1033–1037.
Chen, M.Y., Sailor, M.J., 2011. Anal. Chem. 83, 7186–7193.
DasGupta, S., Shelke, S.A., Li, N.S., Piccirilli, J.A., 2015. Chem. Commun. 51, 9034–9037.
De Stefano, L., Rotiroti, L., Rendina, I., Moretti, L., Scognamiglio, V., Rossi, M., D'Auria, S., 2006. Biosens. Bioelectron. 21, 1664–1667.
Derkus, B., Arslan, Y.E., Bayrac, A.T., Kantarcioglu, I., Emregul, K.C., Emregul, E., 2016. Sens. Actuators B Chem. 228, 725–736.
Girardot, M., Gareil, P., Varenne, A., 2010. Electrophoresis 31, 546–555.
Girardot, M., Li, H., Descroix, S., Varenne, A., 2012. Chromatographia 76, 305–312.
Guo, W., Hong, F., Liu, N., Huang, J., Wang, B., Duan, R., Lou, X., Xia, F., 2015. Adv. Mater. 27, 2090–2095.
Jenison, R.D., Gill, S.C., Pardi, A., Polisky, B., 1994. Science 263, 1425–1429.
Jiang, Y., Feng, Y., Su, J., Nie, J., Cao, L., Mao, L., Jiang, L., Guo, W., 2017. J. Am. Chem. Soc. 139, 18739–18746.
Kalz, J., ten Cate, H., Spronk, H.M., 2014. J. Thromb. Thrombolysis 37, 45–55.
Kant, K., Yu, J., Priest, C., Shapter, J.G., Losic, D., 2014. Analyst 139, 1134–1140.
Lazzara, T.D., Mey, I., Steinem, C., Janshoff, A., 2011. Anal. Chem. 83, 5624–5630.
Li, R., Wu, Z., Wangb, Y., Ding, L., Wang, Y., 2016. Biotechnol. Rep. 9, 46–52.
Lin, C., Katilius, E., Liu, Y., Zhang, J., Yan, H., 2006. Angew. Chem. Int. Ed. 45, 5296–5301.
Lin, V.S.-Y., Motesharei, K., Dancil, K.-P.S., Sailor, M.J., Ghadiri, M.R., 1997. Science 278, 840–844.
Majdinasab, M., Hayat, A., Marty, J.L., 2018. Trends Anal. Chem. 107, 60–77.
Mariani, S., Pino, L., Strambin, L.M., Tedeschi, L., Barillaro, G., 2016. ACS Sens 1, 1471–1479.
Mariani, S., Robbiano, V., Strambini, L.M., Debrassi, A., Egri, G., Dahne, L., Barillaro, G., 2018. Nat. Commun. 9, 5256.
Modh, H., Witt, M., Urmann, K., Lavrentieva, A., Segal, E., Scheper, T., Walter, J.G., 2017. Talanta 172, 199–205.
Mu, D., Liu, Z.-S., Huang, C., Djilali, N., 2007. Microfluid. Nanofluidics 4, 257–260.
Nierodzik, M.L., Karpatkin, S., 2006. Cancer Cell 10, 355–362.
Pacholski, C., Sartor, M., Sailor, M.J., Cuni, F., Miskelly, G.M., 2005. J. Am. Chem. Soc. 127, 11636–11645.
Sambrano, G.R., Weiss, E.J., Zheng, Y.-W., Huang, W., Coughlin, S.R., 2001. Nature 413, 74–78.
Shuman, M.A., Majerus, P.W., 1976. J. Clin. Investig. 58, 1249–1258.
Sun, D., Lu, J., Luo, Z., Zhang, L., Liu, P., Chen, Z., 2018. Biosens. Bioelectron. 120, 8–14.
Sze, J.Y.Y., Ivanov, A.P., Cass, A.E.G., Edel, J.B., 2017. Nat. Commun. 8, 1–10.
Tan, S.Y., Acquah, C., Tan, S.Y., Ongkudon, C.M., Danquah, M.K., 2017. Process Biochem. 60, 42–51.
Tan, Z.J., Chen, S.J., 2006. Biophys. J. 91, 518–536.
Tang, Y., Zhen, L., Liu, J., Wu, J., 2013. Anal. Chem. 85, 8.
Tasset, D., Kubik, M., Steiner, W., 1997. J. Mol. Biol. 272, 688–698.
Tripathy, D., Sanchez, A., Yin, X., Luo, J., Martinez, J., Grammas, P., 2013. Front. Aging Neurosci. 5, 1–9.
Umrao, S., Jain, V., Anusha, Chakraborty, B., Roy, R., 2018. Sens. Actuators B Chem. 267, 294–301.
Urmann, K., Arshavsky-Graham, S., Walter, J.G., Scheper, T., Segal, E., 2016. Analyst 141, 5432–5440.
Urmann, K., Walter, J.G., Scheper, T., Segal, E., 2015. Anal. Chem. 87, 1999–2006.
Vilensky, R., Bercovici, M., Segal, E., 2015. Adv. Funct. Mater. 25, 6725–6732.
W, B., B, H., H, A., M, S., I, L., 1979. Thromb. Haemost. 42, 11.
Wang, Y., Liu, B., 2009. Langmuir 25, 12787–12793.
Xiao, Y., Lubin, A.A., Heeger, A.J., Plaxco, K.W., 2005. Angew. Chem. Int. Ed. 44, 5456–5459.
Yunlong, B., Qiang, Z., 2017. Anal. Methods 9, 5684–5690.
Zhao, Y., Gaur, G., Mernaugh, R.L., Laibinis, P.E., Weiss, S.M., 2016. Nanoscale Res. Lett. 11, 395.
Zhao, Y., Gaur, G., Retterer, S.T., Laibinis, P.E., Weiss, S.M., 2016. Anal. Chem. 88, 10940–10948.
Zou, M., Chen, Y., Xu, X., Huang, H., Liu, F., Li, N., 2012. Biosens. Bioelectron. 32, 148–154.